Journal of Applied Physics

RESEARCH ARTICLE | APRIL 04 2024

Impact of laser energy density on engineering resistive switching dynamics in self-rectifying analog memristors based on $BiFeO_3$ thin films

Xianyue Zhao ; Kefeng Li; Ziang Chen; Jan Dellith ; Andrea Dellith ; Marco Diegel ; Daniel Blaschke ; Stephan Menzel ; Ilia Polian ; Heidemarie Schmidt ; Nan Du

J. Appl. Phys. 135, 135303 (2024)
https://doi.org/10.1063/5.0196718

Journal of Applied Physics ARTICLE pubs.aip.org/aip/jap

Impact of laser energy density on engineering resistive switching dynamics in self-rectifying analog memristors based on $BiFeO_3$ thin films

Cite as: J. Appl. Phys. **135**, 135303 (2024); doi: 10.1063/5.0196718
Submitted: 9 January 2024 · Accepted: 17 March 2024 ·
Published Online: 4 April 2024

View Online Export Citation CrossMark

Xianyue Zhao,[1,2] Kefeng Li,[1,2] Ziang Chen,[1,2] Jan Dellith,[3] Andrea Dellith,[3] Marco Diegel,[3] Daniel Blaschke,[2] Stephan Menzel,[4] Ilia Polian,[5] Heidemarie Schmidt,[1,2] and Nan Du[1,2,a)]

AFFILIATIONS

[1]Institute for Solid State Physics, Friedrich Schiller University Jena, Jena, Germany
[2]Department of Quantum Detection, Leibniz Institute of Photonic Technology (IPHT), Jena, Germany
[3]Department of Competence Center for Micro- and Nanotechnologies, Leibniz Institute of Photonic Technology (IPHT), Jena, Germany
[4]Peter Grünberg Institut (PGI-7), Forschungszentrum Juelich GmbH, Juelich, Germany
[5]Institute of Computer Science and Computer Engineering, University of Stuttgart, Stuttgart, Germany

[a)]**Author to whom correspondence should be addressed:** nan.du@uni-jena.de

ABSTRACT

This study explores the feasibility of precisely tuning the resistive switching behavior of $Au/BiFeO_3/Pt/Ti/SiO_2/Si$ memristors through controlled modulation of laser energy density during pulsed laser deposition (PLD). By systematically reducing the laser energy density within the fabrication process, notable alterations in the properties of the $BiFeO_3$ (BFO) thin film are observed. As the laser energy density decreases, the grain size in the BFO film and the thickness of the film decrease. Furthermore, we obtain the minute structural variations in response to the diverse laser energy densities employed during the deposition process. Energy-dispersive x-ray spectroscopy analysis is employed to investigate the distribution of Ti^{4+} ions within the BFO thin film. The reduction in the grain size and film thickness, along with the prominent nucleation of specifically oriented grains, and the diffusion of Ti^{4+} ions, lead to the BFO memristor fabricated with a lower laser energy density having more grain boundaries and a shortened conduction path (grain boundary) in the thickness direction. Consequently, the enhanced movement of oxygen vacancies facilitates their preferential accumulation along the grain boundaries within the BFO layer, resulting in an augmented on/off ratio, rectification factor, and set current in the devices. Overall, our findings explain the significant influence of laser energy density in PLD on the microstructure and electrical properties of BFO thin films. Particularly, the lower energy densities are employed to improve electrical characteristics. This research not only enhances our fundamental understanding but also provides valuable insights into optimizing BFO memristors for reliable, robust, and practical applications.

I. INTRODUCTION

Memristors have garnered significant attention in the field of electronics due to their potential for revolutionizing memory storage, neuromorphic computing, and logic circuitry.[1–4] Among various memristive materials, bismuth ferrite (BFO) stands out as a promising candidate for analog resistive switching[5–8] and for digital resistive switching[9–12] owing to its multiferroic nature that exhibits both ferroelectric and antiferromagnetic properties. Analog resistive switching memristors are crucial for neuromorphic computing and artificial intelligence, where the ability to perform synaptic weight updates is essential for emulating the brain's cognitive processes.

Researchers have been exploring two main avenues to optimize the performance of BFO memristors in practical applications. First, they are focused on improving integration and signal modulation strategies at the application level, including increasing crossbar density, signal frequency, and exploring multi-level bit generation.[13–16] Second, attention is directed toward material technology advancements, involving different electrodes, substrate materials, additional layers, doping, and fabrication parameter control.[17–21] Notably, material technology advancements serve as the fundamental catalyst for improving performance, underpinning the overall functionality and potential of BFO memristors.

Pulsed laser deposition (PLD) stands as a prominent technique in the preparation of BFO memristors, making it a pivotal focus within materials technology for enhancing memristor performance.[22] Several studies have aimed to enhance the performance of memristors by systematically manipulating various parameters of PLD, including laser energy density, laser frequency, oxygen pressure, substrate temperature, and annealing conditions.[23–27] These studies have demonstrated the crucial influence of PLD parameters on the morphology and electrical properties of BFO thin films, highlighting the potential for optimizing these parameters to achieve customized memristor performance. However, limited research has been conducted specifically on the improvement of BFO memristors using PLD techniques. Lamichhane *et al.*[27] report on the influence of laser energy density on BFO-based memristor. Significantly, our self-rectifying analog BFO memristor exhibits distinct characteristics compared to Lamichhane's BFO memristor, including unique electrode materials and mechanisms. However, it is important to note that our self-rectifying BFO memristors are known for their electroforming-free operation. This means that these memristors do not require a separate forming step to initialize the device. As a result, the impact of laser fluence on the BFO layer in our memristor may vary considerably.

This study aims to investigate the influence of laser energy density on the morphology and electrical properties of BFO memristors. We report a comprehensive analysis, examining the effects of varying laser energy density on key parameters such as maximum set current, leakage current, resistance ratio, and rectification factor. A deeper understanding of the relationship between laser energy density and the resistive switching (RS) behavior of BFO memristors can be obtained by systematically characterizing these properties. Various characterization techniques are used to observe the changes in surface morphology and internal structure to the effect of RS behaviors. These changes, including the decrease in grain size and film thickness, along with the nucleation of specifically oriented grains and diffusion of Ti^{4+} ions, contribute to the presence of more grain boundaries and shortened conduction paths in the BFO memristor with lower laser energy density. Consequently, this promotes the enhanced movement of oxygen vacancies, leading to their preferential accumulation along the grain boundaries within the BFO layer. These structural variations result in improved device performance, manifested by an increased on/off ratio, rectification factor, and set current in the memristor devices.

The results of this investigation contribute to the understanding of how laser energy density influences RS behavior and highlight the importance of tailoring memristor properties for specific applications. By fine-tuning the laser energy density, it becomes possible to achieve lower power consumption, improved energy efficiency, enhanced reliability, and better rectifying behavior. The optimization of BFO memristor characteristics through laser energy density control opens up new avenues for the realization of high-performance and energy-efficient electronics.

This paper is structured as follows: Sec. II investigates the method of BFO preparation and the equipment and parameters used for BFO morphology measurements. Section III provides a comprehensive analysis of the morphological and material structures of amnesic resistors fabricated under various laser energy densities. It examines the underlying reasons and connections that contribute to their diverse RS behavior. Additionally, the section proposes an adaptive scheme for tailoring the RS behavior based on specific application requirements through the utilization of different laser energy densities. Finally, Sec. IV discusses a comprehensive summary of our findings, including the morphological and material structures of the memristors fabricated with different laser energy densities and discusses potential avenues for future improvements.

II. EXPERIMENTAL SECTION

To fabricate the BFO-based memristors, we employ PLD to deposit BFO thin films on a Pt/Ti bottom electrode (BE) with a SiO_2/Si substrate. The growth conditions for the BFO thin film deposition are determined based on previous studies.[6] The frequency of the laser pulses is set at 10 Hz, and the deposition pressure is maintained at 1.3×10^{-2} mbar. The deposition process is carried out at a substrate temperature of 650 °C. Different laser energy densities are utilized during the deposition process, specifically 2.1, 2.3, 2.5, and 2.6 J/cm^2. DC magnetron sputtering through a metal shadow mask is used to deposit the top electrode (TE) with a circular structure. Sputtering is carried out with a power of 100 W at a pressure of 2.6 Pa with argon as the sputtering gas. The resulting thickness of Au is approximately 180 nm, and the area of the TE is maintained at approximately $4.52\times10^4\,\mu m^2$(120 μm diameter). This electrode configuration ensures proper electrical contact and allows for the desired electrical measurements and characterization of the memristors.

Atomic force microscopy (AFM) is carried out using a VistaScope system provided by Molecular Vista Inc., employing gold-coated AFM tips from nanosensors (SD-NCHAu25-W) with a resonance frequency of approximately 250 kHz. The AFM images are captured in tapping mode at the second mechanical resonance of the cantilevers, using a tapping amplitude of 1 nm and a set point of 85 %. A second-order line-by-line mode in the scan direction is used to level the images. The root mean square (RMS) roughness is determined using SurfaceWorks version 3.0 release; 30 and 5 images are taken for each memristor to ensure statistical relevance. The arithmetic average and standard deviation of the RMS roughness and grain size are computed. For the calculation of grain sizes, a watershed algorithm is utilized in the Gwyddion software version 2.60 after marking the structures.

The thicknesses of the BFO thin films are measured by scanning electron microscopy (SEM, system FEI Helios NanoLab G3 UC). The structural characteristics of the BFO films are studied using energy dispersive x-ray spectroscopy (EDX). The EDX spectra are taken using a Silicon Drift Detector (SDD; 60 mm^2) XFlash 5130 from BRUKER Nano GmbH, Berlin, Germany. The crystallinity of the films on quartz substrates is characterized by grazing x-ray diffraction (giXRD, Panalytical X'Pert Pro) with Cu-K$\alpha_{1,2}$ (Kα1: 0.154 06 nm) radiation.

The resulting memristors are investigated at room temperature on a stand for measuring the current–voltage (I–V) characteristics of memristors using a Keithley 2400 two-channel generator/meter with a two-probe positioning system in the applied voltage bipolar mode.

III. RESULTS AND DISCUSSION

A. Resistive switching mechanism

The I–V curve is measured by applying a triangular sweeping bias with an amplitude of $|V_m| = 10\,V$. Figure 1(a) illustrates the switching directions of the I–V curve, which are as follows: $0\,V \rightarrow +V_m \rightarrow 0\,V \rightarrow -V_m \rightarrow 0\,V$. During the entire sweeping process, a total of 101 voltage steps are taken at 0.1 V/step, and the pulse width for each step is set at 100 ms. The I–V curve demonstrates analog bipolar RS behavior in BFO memristors. By applying a positive sweeping bias with an amplitude of $+10\,V$, the low resistance state (LRS) can be achieved, while a negative sweeping bias with an amplitude of $-10\,V$ is used to achieve the high resistance state (HRS). The resistance values in the LRS and HRS of the BFO memristor are determined at a reading voltage of $+2\,V$ and can be recorded as R_{HRS} and R_{LRS}, respectively. The on/off ratio of the BFO memristor can be calculated as R_{HRS}/R_{LRS}.

During the pulsed laser deposition (PLD) process, the BFO thin film is deposited in an atmosphere with an oxygen pressure of 1.3×10^{-2} mbar, which leads to the generation of a considerable quantity of defects in the BFO thin film. Consequently, numerous randomly distributed oxygen vacancies exist in the BFO thin film, rendering the BFO layer as an n-type semiconductor. The BFO film forms two Schottky barriers when in contact with the Au TE and Pt BE, which exist at the Au/BFO interface and the BFO/Pt interface, respectively.

The RS mechanism of the BFO memristor can be attributed to the movement of $V_o^{\cdot\cdot}$ in the BFO thin film when applying the bias with different polarities to the TE. When a large positive writing bias is applied to the TE, $V_o^{\cdot\cdot}$ are pushed toward the BE direction and accumulate in the BE region. The drifting of $V_o^{\cdot\cdot}$ in the BFO thin film is schematically demonstrated on the right side of the I–V curve in Fig. 1(a). Due to the accumulated $V_o^{\cdot\cdot}$ at the BFO/Pt interface, the Schottky barrier is lowered.

The equivalent circuit on the right side of the I–V curve in Fig. 1(a) shows one forward-biased diode (D_{TE}) at the Au/BFO interface while the BFO/Pt interface Schottky barrier is modeled as a resistor (R_{BE}). Another resistor (R_i) represents the bulk resistance of the BFO thin film. Applying a large positive writing bias results in the forward biasing of the diode (D_{TE}), allowing a high current to flow through the memristor stack, as depicted on the right side of the I–V curve in Fig. 1(a). When a negative writing bias is applied to the TE, the mobile donors $V_o^{\cdot\cdot}$ drift toward the TE, leading to the formation of a Schottky barrier at the BFO/Pt interface. The drifting of $V_o^{\cdot\cdot}$ is schematically demonstrated on the left side of the I–V curve in Fig. 1(a). In the high resistance state (HRS), the equivalent circuit of the memristor can be represented by a head-to-head diode configuration consisting of two diodes (D_{TE} and D_{BE}) connected in an anti-series arrangement. Regardless of the polarity of the bias, the Schottky barrier at the BFO/Pt interface (D_{BE}) or the Schottky barrier at the Au/BFO interface (D_{TE}) blocks the current flow through the memristor stack. The diode behavior observed in the Au/BFO/Pt structure can be attributed to the interplay of the individual Schottky contacts at the Au/BFO and BFO/Pt interfaces within the memristor stack. The reduction of the Schottky barrier at the BFO/Pt bottom interface leads to the establishment of an Ohmic contact, while an increase in the Schottky barrier at the Au/BFO top interface occurs due to the accumulation of donors at the bottom interface. Upon application of a positive reading bias, the diode D_{TE} becomes forward biased, resulting in the LRS of the MIM structures. Subsequent application of a negative writing bias causes the mobile oxygen vacancy donors to be released from the deep potential wells and drift toward the top electrode. Consequently, the Schottky barrier at the BFO–Pt bottom interface is reinstated, resetting the MIM structure to the HRS.

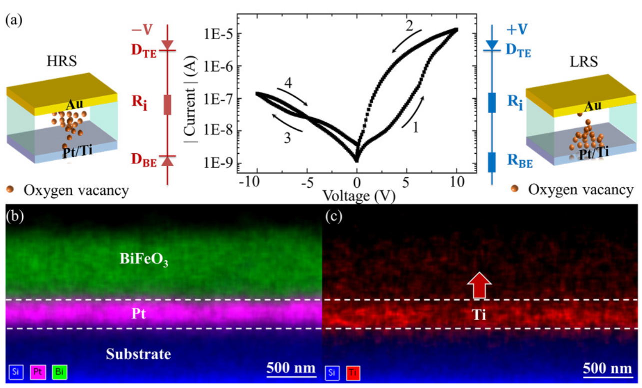

FIG. 1. (a) I–V curve of BFO memristor and schematic image of BFO memristor switching mechanism. On the left and right side of I–V curve show the $V_o^{\cdot\cdot}$ and corresponding equivalent circuits in HRS and LRS, with illustrations of drift and diffusion currents. (b) EDX image of BFO memristor prepared at laser energy density of 2.1 J/cm^2, and (c) displays the Ti distribution.

B. Morphology

EDX analysis confirms the presence and diffusion of Ti within the BFO layer. It should be pointed out that according to the research of You *et al.*,[7] in the BFO thin film, $V_o^{\cdot\cdot}$ serve as mobile donors, while Ti^{4+} ions act as fixed donors near the BFO/Pt interface. The EDX spectra in Figs. 1(b) and 1(c) clearly show the BFO layer, Pt/Ti BE, and SiO_2/Si substrate of the BFO memristor from top to bottom, where Ti^{4+} ions are represented in red.

As depicted in Fig. 1(c), Ti^{4+} ions have diffused into the BFO film due to the BFO being deposited at a high temperature (substrate temperature of 650 °C). The deposition process with ambient heating provokes the substitutional incorporation of Ti donors into the BFO lattice, resulting in a rectifying/non-rectifying contact with a flexible barrier height near the BE region. Ti^{4+} ions are used to substitute some Fe ions in BFO due to the closed ionic radius of Ti^{4+} and Fe^{3+} (0.68 and 0.65 Å, respectively).[7]

Figure 2(a) presents the I–V characteristics of BFO memristors fabricated with varying laser energy densities: 2.1, 2.3, 2.5, and 2.6 J/cm^2. These memristors are subjected to the same sweeping bias conditions, employing a triangular waveform with an amplitude of $|V_m| = 10$ V. Notably, the I–V curves exhibit hysteresis, and distinct variations are observed across different laser energy densities.

The resistance ratios, obtained by calculating the ratio of resistances in the sweeping bias from −10 to +10 V to the resistances in the sweeping bias from +10 to −10 V, are illustrated in Fig. 2(b). A discernible trend in the resistance ratio is observed in the positive bias range for each laser energy density. Initially, an increase in resistance ratio is observed, followed by a subsequent decrease. Decreasing the laser energy density results in a significant improvement in the resistance ratio within the positive bias range. At laser energy densities of 2.1, 2.3, 2.5, and 2.6 J/cm^2, the BFO memristors exhibit maximum resistance ratios of 58, 46, 22, and 7, respectively, at corresponding voltage values of 3.4, 4.1, 4.2, and 3.3 V. The on/off ratios of the BFO memristor at +2 V are 30, 13, 6, and 3 for laser energy densities of 2.1, 2.3, 2.5, and 2.6 J/cm^2, respectively.

The increased resistance ratio and on/off ratio observed at lower laser energy densities can be attributed to a more significant decrease in resistance during the sweeping bias from +10 to 0 V compared to the sweeping bias from 0 to +10 V. However, no significant correlation between resistance and laser energy density is observed within the negative bias range, likely due to the absence of notable differences in resistance values between the sweeping bias from 0 to −10 V and the sweeping bias from −10 to 0 V.

Figure 2(c) illustrates the thickness dependence with respect to laser energy density, while the corresponding SEM images are presented in Fig. 2(d). Each SEM image showcases the BFO layer, Pt/Ti BE, and SiO_2/Si substrate. A noticeable trend in the thickness of the BFO thin film is observed as the laser energy density decreases [Fig. 2(c)]. This can be attributed to the reduced size of ablated BFO grains and fewer particulates deposited on the film.[28,29] Consequently, the overall current flowing through the BFO memristor may decrease due to the reduced thickness. This can be attributed to the effect of a thinner BFO layer, which leads to a larger effective electric field across the memristive stack when the same external bias is applied.

Figure 3(a) presents images obtained from an atomic force microscope (AFM) of deposited BFO thin films with varying laser energy densities ranging from 2.1 to 2.6 J/cm^2, scanned over a surface area of $5 \times 5\,\mu$m. The surface morphology of the BFO thin film prepared at a laser energy density of 2.1 J/cm^2 is depicted in Fig. 3(b), revealing an average grain size of approximately 2.5×10^5 nm^2. As the laser energy density increases to 2.6 J/cm^2, the average grain size expands to $2.8{\times}10^5$ nm^2. Note the kinetic energy of the particles ejected from the target increases with the laser energy density in the PLD process, causing the particles to accumulate and form larger crystalline structures upon reaching the substrate, as has been demonstrated in other oxide semiconductor materials.[28,30,31]

The RMS roughness of the BFO films, as shown in Fig. 3(c), remains relatively constant for laser energy densities of 2.1, 2.3, and 2.5 J/cm^2, with a noticeable increase observed only at a laser energy density of 2.6 J/cm^2. This observed increase in surface roughness at a laser energy density of 2.6 J/cm^2 can be possibly attributed to the larger grain size and increased aggregation of nanoparticles.

Figure 3(d) presents background-subtracted giXRD patterns (2θ-scan with omega = 5°) for the corresponding memristors, confirming the successful formation of polycrystalline BFO thin films. The primary BFO peaks are identified based on their Miller indices, including (0 1 2), (1 0 4), (0 0 6), (0 2 4), (1 1 6), (0 1 8), and (2 1 4) (ICSD reference card, collection code 417 304). As depicted in Fig. 3(d), increasing the laser energy density results in a decrease in the intensity of the diffraction peaks (0 1 2) and (0 2 4),

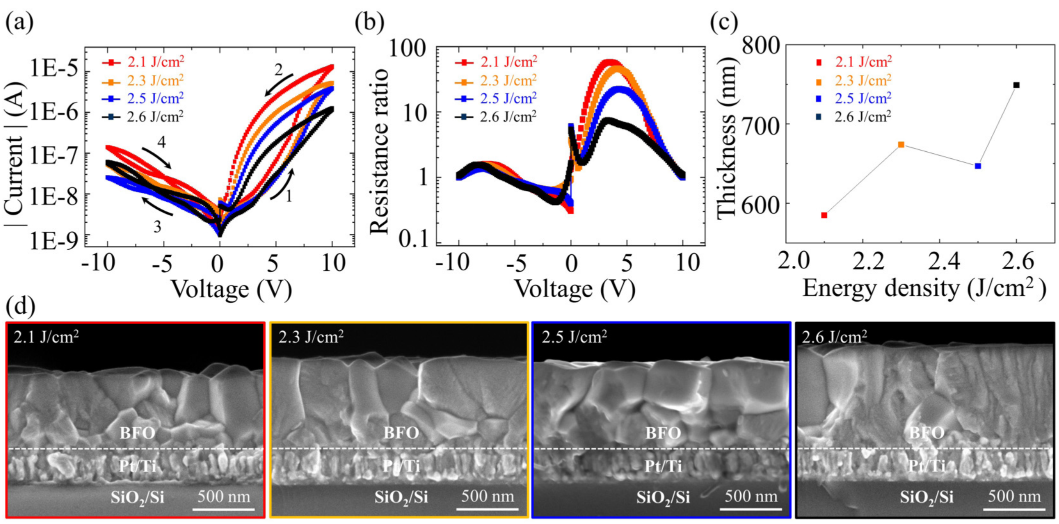

FIG. 2. Electrical and structural properties of BFO memristor and thin films prepared at different laser energy densities. (a) I–V characteristics of BFO memristor under various laser energy densities. (b) Resistance ratio of BFO memristor fabricated under various laser energy densities. (c) Thickness of BFO thin films as a function of laser energy density. (d) SEM images of BFO thin films prepared at different laser energy densities: 2.1, 2.3, 2.5, and 2.6 J/cm^2.

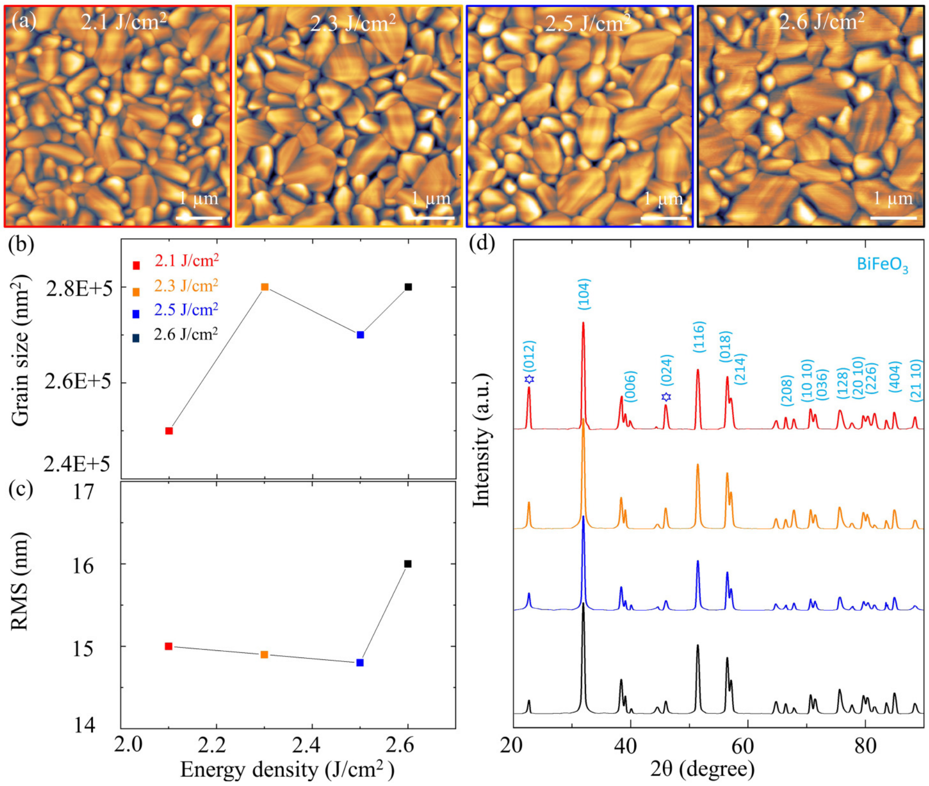

FIG. 3. AFM images of BFO thin films prepared using different laser energy densities: (a) 2.1, 2.3, 2.5, and 2.6 J/cm^2. The dependence of grain size and RMS roughness on laser energy density is illustrated in (b) and (c), respectively. Background-subtracted giXRD patterns of BFO thin films prepared at various laser energy densities are presented in (d).

whereas the other orientations have similar intensities for the used laser fluences. A plausible conjecture emerges regarding a potential correlation between these (0 1 2) crystallites and the movement of oxygen vacancies within the memristor cell. Higher intensities of (0 1 2) crystal orientations might correspond to the enhanced movement of oxygen vacancies, consequently yielding lower resistance in the memristor. The underlying mechanism for this phenomenon remains unclear. The mobility of oxygen vacancies may be influenced by the number and/or size of these crystallites and/or their grain boundaries. Further investigation is warranted to elucidate the intricate dynamics underlying this observed behavior.

C. Electrical properties

The electrical properties of the BFO memristor are investigated under different laser energy densities, including the set current (I_{max+}), leakage current (I_{max-}), resistance ratio, and rectification factor. Figure 2(a) presents the observed variations in the I–V behaviors of a single cell for different laser energy densities, and the investigation is extended by analyzing the I–V behavior of 50 individual cells for each laser energy density in Fig. 4. The maximum amplitude of the applied voltage is $|V_m| = 10$V for all measurements.

In Figs. 4(a) and 4(b), the average set current (I_{max+}) and leakage current (I_{max-}) obtained from 50 cells for each laser energy density are presented. It is observed that as the laser energy density decreases, the set current (I_{max+}) significantly increases. In contrast, the leakage current (I_{max-}) shows a slight increase. The conduction mechanism model of the memristor suggests that ion dynamics modify electron transport across the active electrode/oxide interface. Although the model does not explain resistive switching dynamics, it is clear that ion dynamics and electronic conduction are closely related.[32] In a BFO memristor, electronic conduction primarily relies on the migration of oxygen vacancies, significantly impacting the material's electrical behavior. The movement of oxygen vacancies, which predominantly occurs along the grain boundaries, influences the electronic conduction behavior. It has been shown that in the presence of metallic electrodes, the movement of oxygen from the grain boundary (GB) to the electrodes is energetically favored, leaving the GB oxygen-poor. The formation energies of the metal atoms located at the interstitial positions of the GB are also negative with respect to their metallic phase, favoring their migration from the electrodes or metal-rich clusters to the GBs. In addition, the accumulation of metal atoms in the GB may make it metallic, providing conduction paths between the electrodes. Therefore, the GB facilitates both the formation of oxygen vacancies and the incorporation of reactive metals in the oxide.[33] The shorter conduction path (grain boundary) in the thickness direction leads to an increased set current (I_{max+}) as the laser energy density decreases.

The resistance changes in the Au/BFO/Pt structure can be primarily attributed to the movement of oxygen vacancies at the interface. For films prepared with a laser energy density of 2.1 J/cm^2, the oxygen vacancies are assumed to possess increased movement velocity and tend to accumulate more readily along the grain

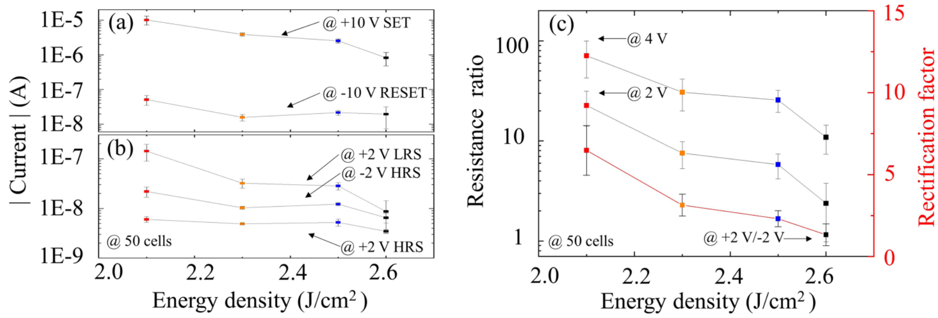

FIG. 4. Electrical properties of BFO memristor fabricated under various laser energy densities. (a) illustrates the set and reset (leakage) currents at +10 and −10 V, respectively, presenting the averaged results obtained from 50 cells. (b) shows LRS current at +2 V, HRS current at −2 V, and HRS current at +2 V are presented as the average results obtained from 50 cells. (c) resistance ratio at +2 V, resistance ratio at +4 V, and rectification factor are presented as the average results obtained from 50 cells.

boundaries within the BFO layer during the set or reset process. One possibility is a change in film density, which affects the mobility of $V_o^{\cdot\cdot}$. Another possibility is the field acceleration of the transport due to the thinner film at 2.1 J/cm^2. Consequently, there is an increased likelihood for the vacancies to migrate and concentrate between the top and bottom interfaces of the memristor, resulting in a more significant change in current during the RS process. Note that the higher defect concentration and the conductive region near the grain boundaries, due to the higher concentration of Ti^{4+} ions at the BE region, may contribute to changes in the conduction regime and resistance.

In practical applications, it is desirable to minimize the set current (I_{max+}) and leakage current (I_{max-}) while maintaining a high on/off ratio to reduce energy consumption and improve energy efficiency. Figure 4(b) presents the current values obtained from sweeping biases of +10 to 0, 0 to −10, and 0 to +10 V at a sweep bias of +2 and −2 V. As the laser energy density decreases, the current value at +2 V from the sweeping bias of +10 to 0 V decreases, while the current values at +2 V from the sweeping bias of 0 to −10 V and the current value at +2 V from the sweeping bias of 0 to +10 V tend to fluctuate.

The resistance ratio, calculated in the same manner as for the single cell, reflects the average results from 50 cells. In Fig. 4(b), the black curves show the relationship between laser energy density and resistance ratio. It can be observed that as the laser energy density decreases, the resistance ratio significantly increases. At +2 V, the resistance ratio increases from 3 to 23, while at +4 V, it increases from 11 to 72. The rectification factor is defined as the relative enhancement of the current at +2 V in the sweeping bias from +10 to 0 V (forward-biased) compared to the current at +2 V in the sweeping bias from 0 to −10 V (reverse-biased). The red curve in Fig. 4(b) represents the variation of the rectification factor, which shows an increasing trend from 2 to 7 as the laser energy density decreases. A higher rectification factor and resistance ratio provide a better rectifying effect and reduce the occurrence of sneak path parasitic effects in passive crossbar arrays.

Overall, the electrical properties of the BFO memristor, including the set current, leakage current, resistance ratio, and rectification factor, are influenced by the laser energy density. Decreasing the laser energy density results in an increase in the set current and resistance ratio, while the leakage current slightly increases. These variations can be attributed to the role of grain boundaries, oxygen vacancies and the formation of conductive paths. Minimizing the set current and leakage current while maintaining a high resistance ratio and rectification factor is beneficial for reducing energy consumption and improving the efficiency of BFO memristor devices.

D. Discussion

Our comprehensive investigation of the morphology and electrical properties of the BFO memristor under different laser energy densities provides valuable insights into the RS behavior. Optimizing various memristor properties is possible by controlling the laser energy density during fabrication. It is important to note that different applications have specific requirements for BFO memristor properties. For non-volatile memory applications, high switching ratios and large resistance ratios are desired to ensure precise signal control. Artificial synapses benefit from minimized power consumption, making lower set currents and leakage currents desirable. Logic circuits, on the other hand, benefit from higher rectification factors for efficient signal processing.

By optimizing the set current, leakage current, resistance ratio, and rectification factor, the overall performance of BFO memristors can be enhanced, meeting the specific needs of different applications such as non-volatile memory, artificial synapses, and logic circuits. Increasing the laser energy density results in a smaller set current (applied at +10 V), leading to lower power consumption and improved energy efficiency. This reduction in set current is beneficial for applications where energy saving is a priority.

Additionally, increasing the laser energy density decreases leakage current (measured at −10 V), effectively suppressing sneak paths and enhancing the accuracy of analog memory operations. By reducing leakage current, the memristor exhibits more reliable and precise RS behavior. Decreasing the laser energy density results in a larger on/off ratio, which enables better differentiation between different resistance levels. This larger on/off ratio enhances the functionality of the memristor by allowing for more distinct and reliable resistance states. Furthermore, decreasing the laser energy density results in a higher rectification factor, indicating improved rectifying behavior. This is particularly important for applications such as logic circuits, where efficient signal processing and logic operations rely on a high rectification factor.

It should be noted that this study does not cover discussions on C2C (Chip-to-Chip) and D2D (Device-to-Device) communication, endurance, and retention in BFO memristor applications. Further investigation and analysis may be necessary to fully understand the implications of these aspects.

Apart from laser energy density, there are several parameters during the process of pulsed laser deposition that can be adjusted to improve the performance of BFO, with temperature and pressure being particularly significant. Substrate temperature and oxygen pressure are vital parameters in PLD, each affecting the nucleation, growth kinetics, and crystallinity of deposited films. For instance, variations in substrate temperature during deposition can significantly impact the film's microstructure and crystalline phase formation. Similarly, adjusting deposition pressure alters the nucleation density and surface morphology of the films, consequently influencing their electrical and magnetic properties. In a study by Jiang *et al.*,[34] varying the surface morphology of the BFO thin film is sensitive to substrate temperature and oxygen pressure rather than laser energy density. When the substrate temperature deviates within a narrow range, either excessively high or low, it invariably leads to elevated RMS roughness due to the formation of parasitic phases such as Bi_2O_3 or Fe_2O_3. The presence of these impurities significantly impacts the RS behavior of the BFO memristor. Similarly, variations in oxygen pressure within a narrow range also exert a predominant influence on the surface morphology of the BFO film, consequently affecting the RS behavior of the memristor. This comparison underscores the overarching significance of laser energy density in shaping the properties of the BFO film, surpassing the effects of temperature and oxygen pressure adjustments. Notably, based on our study laser energy density offers precise control over RS behavior while concurrently mitigating RMS, thereby underscoring its advantage in this context.

IV. CONCLUSION

In this study, we report an investigation on the RS behavior of BFO memristors fabricated using PLD, focusing on the influence of laser energy density. By systematically varying the laser energy density within the range of 2.1–2.6 J/cm^2, we can achieve controlled tuning of various RS properties of the memristors. Specifically, we analyze and observe changes in the set current, leakage current, resistive ratio, and rectification factor in response to the different laser energy densities employed.

To obtain a comprehensive understanding of the memristor characteristics, a variety of characterization techniques are employed, allowing for a detailed examination of the microstructure of the BFO thin films. The morphology of the BFO films is analyzed using AFM, providing insights into the grain size and surface roughness. SEM is employed to investigate the thickness of the BFO thin film. It reveals a decrease in thickness as the laser energy density decreases. To analyze the distribution of Ti^{4+} ions within the BFO thin film, EDX is performed. EDX provides insights into the elemental composition and distribution of Ti^{4+} ions within the BFO thin film. Furthermore, giXRD measurements are conducted to confirm the successful formation of polycrystalline BFO thin films. The electrical properties are evaluated through current–voltage measurements, enabling the determination of parameters such as set current, leakage current, resistance ratio, and rectification factor.

The findings reveal a significant correlation between the laser energy density and the film's microstructure. Specifically, the thin film with a lower energy density has more grain boundaries and shortened conduction paths in the film thickness direction. This results in improved electrical properties, particularly higher on/off ratios. It is important to note that additional research is necessary to investigate other factors that can enhance the performance of BFO memristors. This includes exploring different TE materials, doping of the BFO thin film, and other parameters related to the PLD process. By considering these additional factors, we can further enhance the characteristics of BFO memristors and advance their potential for various applications.

ACKNOWLEDGMENTS

X.Z., K.L., and N.D. acknowledge the funding by German Research Foundation (DFG) Project MemDPU (Grant No. DU 1896/3-1). Z.C. and N.D. acknowledge the funding by German Research Foundation (DFG) Project MemCrypto (Grant No. DU 1896/2-1). S.M. acknowledges the funding by German Research Foundation (DFG) Project MemDPU (Grant No. ME 4612/1-1). I.P. acknowledges the funding by German Research Foundation (DFG) Project MemCrypto (Grant No. PO 1220/15-1). All coauthors acknowledge the fruitful discussions with Danilo Bürger, Ilona Skorupa, and Hans-Jürgen Engelmann from Helmholz-Zentrum Dresden-Rossendorf (HZDR) regarding the switching mechanism on the BFO memristor.

AUTHOR DECLARATIONS

Conflict of Interest

The authors have no conflicts to disclose.

Author Contributions

Xianyue Zhao: Data curation (equal); Formal analysis (equal); Investigation (equal); Methodology (equal); Writing – original draft (equal). **Kefeng Li:** Data curation (supporting); Formal analysis (supporting). **Ziang Chen:** Data curation (supporting); Formal analysis (supporting). **Jan Dellith:** Formal analysis (supporting); Investigation (supporting). **Andrea Dellith:** Formal analysis (supporting); Investigation (supporting). **Marco Diegel:** Data curation (supporting); Formal analysis (supporting); Investigation (supporting); Writing – review & editing (supporting). **Daniel Blaschke:** Data curation (supporting); Investigation (supporting). **Stephan Menzel:** Formal analysis (supporting); Investigation (supporting); Methodology (supporting); Writing – review & editing (supporting). **Ilia Polian:** Writing – review & editing (supporting). **Heidemarie Schmidt:** Conceptualization (supporting); Methodology (supporting); Writing – review & editing (supporting). **Nan Du:** Conceptualization (equal); Formal analysis (equal); Funding acquisition (equal); Investigation (equal); Methodology (equal); Writing – original draft (equal); Writing – review & editing (equal).

DATA AVAILABILITY

The data that support the findings of this study are available from the corresponding author upon reasonable request.

REFERENCES

[1] W. Lu, K.-H. Kim, T. Chang, and S. Gaba, "Two-terminal resistive switches (memristors) for memory and logic applications," in *16th Asia and South Pacific Design Automation Conference (ASP-DAC 2011)* (IEEE, 2011), pp. 217–223.

[2] S. Stathopoulos, A. Khiat, M. Trapatseli, S. Cortese, A. Serb, I. Valov, and T. Prodromakis, "Multibit memory operation of metal-oxide Bi-layer memristors," Sci. Rep. **7**, 17532 (2017).

[3] S. Wen, X. Xie, Z. Yan, T. Huang, and Z. Zeng, "General memristor with applications in multilayer neural networks," Neural Netw. **103**, 142–149 (2018).

[4] K. Sun, J. Chen, and X. Yan, "The future of memristors: Materials engineering and neural networks," Adv. Funct. Mater. **31**, 2006773 (2021).

[5] Y. Shuai, S. Zhou, D. Bürger, M. Helm, and H. Schmidt, "Nonvolatile bipolar resistive switching in Au/$BiFeO_3$/Pt," J. Appl. Phys. **109**, 124117 (2011).

[6] T. You, N. Du, S. Slesazeck, T. Mikolajick, G. Li, D. Bürger, I. Skorupa, H. Stöcker, B. Abendroth, A. Beyer, and K. Volz, "Bipolar electric-field enhanced trapping and detrapping of mobile donors in $BiFeO_3$ memristors," ACS Appl. Mater. Interfaces **6**, 19758–19765 (2014).

[7] T. You, Y. Shuai, W. Luo, N. Du, D. Bürger, I. Skorupa, R. Hübner, S. Henker, C. Mayr, R. Schüffny, and T. Mikolajick, "Exploiting memristive $BiFeO_3$ bilayer structures for compact sequential logics," Adv. Funct. Mater. **24**, 3357–3365 (2014).

[8] N. Du, N. Manjunath, Y. Li, S. Menzel, E. Linn, R. Waser, T. You, D. Bürger, I. Skorupa, D. Walczyk, and C. Walczyk, "Field-driven hopping transport of oxygen vacancies in memristive oxide switches with interface-mediated resistive switching," Phys. Rev. Appl. **10**, 054025 (2018).

[9] S.-W. Chen and J.-M. Wu, "Unipolar resistive switching behavior of $BiFeO_3$ thin films prepared by chemical solution deposition," Thin Solid Films **519**, 499–504 (2010).

[10] J. Luo, S. Lin, Y. Zheng, and B. Wang, "Nonpolar resistive switching in mn-doped $BiFeO_3$ thin films by chemical solution deposition," Appl. Phys. Lett. **101**, 062902 (2012).

[11] S. Hong, T. Choi, J. H. Jeon, Y. Kim, H. Lee, H.-Y. Joo, I. Hwang, J.-S. Kim, S.-O. Kang, S. V. Kalinin, and B. H. Park, "Large resistive switching in ferroelectric $BiFeO_3$ nano-island based switchable diodes," Adv. Mater. **25**, 2339–2343 (2013).

[12] T. Wang, L. Cheng, C. Wang, W. Cheng, H. Wang, H. Sun, J. Chen, and X. Miao, "Deposition temperature and thickness effect on the resistive switching in $BiFeO_3$ films," IEEE Trans. Magn. **56**, 7505004 (2020).

[13] N. Du, M. Kiani, C. G. Mayr, T. You, D. Bürger, I. Skorupa, O. G. Schmidt, and H. Schmidt, "Single pairing spike-timing dependent plasticity in $BiFeO_3$ memristors with a time window of 25 ms to 125 μs," Front. Neurosci. **9**, 227 (2015).

[14] Z. Lu, Z. Fan, P. Li, H. Fan, G. Tian, X. Song, Z. Li, L. Zhao, K. Huang, F. Zhang, and Z. Zhang, "Ferroelectric resistive switching in high-density nanocapacitor arrays based on $BiFeO_3$ ultrathin films and ordered Pt nanoelectrodes," ACS Appl. Mater. Interfaces **8**, 23963–23968 (2016).

[15] N. Yang, Z.-Q. Ren, C.-Z. Hu, Z. Guan, B.-B. Tian, N. Zhong, P.-H. Xiang, C.-G. Duan, and J.-H. Chu, "Ultra-wide temperature electronic synapses based on self-rectifying ferroelectric memristors," Nanotechnology **30**, 464001 (2019).

[16] Y. Zhao, R. Su, L. Cheng, M. Cheng, W. Cheng, H. Tong, H. Sun, J. Yan, and X. Miao, "Ultra-low power consumption and favorable reliability mn-doped $BiFeO_3$ resistance-switching devices via tunable oxygen vacancy," Ceram. Int. **49**, 9090–9096 (2023).

[17] F. Yan, T. Zhu, M. Lai, and L. Lu, "Effect of bottom electrodes on nanoscale switching characteristics and piezoelectric response in polycrystalline $BiFeO_3$ thin films," J. Appl. Phys. **110**, 084102 (2011).

[18] S. Wu, L. Ren, F. Yu, K. Yang, M. Yang, Y. Wang, M. Meng, W. Zhou, and S. Li, "Colossal resistance switching in Pt/$BiFeO_3$/Nb: $SrTiO_3$ memristor," Appl. Phys. A **116**, 1741–1745 (2014).

[19] Z. Peng, F. Wu, L. Jiang, G. Cao, B. Jiang, G. Cheng, S. Ke, K.-C. Chang, L. Li, and C. Ye, "HfO_2-based memristor as an artificial synapse for neuromorphic computing with tri-layer HfO_2/$BiFeO_3$/HfO_2 design," Adv. Funct. Mater. **31**, 2107131 (2021).

[20] R. Su, M. Cheng, A. Dong, Y. Zhao, W. Cheng, R. Yang, J. Yan, and X. Miao, "Interface barrier-induced conversion of resistive switching mechanism in mn-doped $BiFeO_3$ memristor," Appl. Phys. Lett. **121**, 203503 (2022).

[21] Q. Xia, Y. Qin, and P. Qiu, "Power-efficient and highly uniform $BiFeO_3$-based memristors optimized with TiInSnO electrode interfacial effect," Adv. Electron. Mater. **8**, 2200435 (2022).

[22] X. Zhao, S. Menzel, I. Polian, H. Schmidt, and N. Du, "Review on resistive switching devices based on multiferroic $BiFeO_3$," Nanomaterials **13**, 1325 (2023).

[23] K.-C. Liu, W.-H. Tzeng, K.-M. Chang, J.-J. Huang, Y.-J. Lee, P.-H. Yeh, P.-S. Chen, H.-Y. Lee, F. Chen, and M.-J. Tsai, "Investigation of the effect of different oxygen partial pressure to $LaAlO_3$ thin film properties and resistive switching characteristics," Thin Solid Films **520**, 1246–1250 (2011).

[24] K. C. Sekhar, K. Kamakshi, S. Bernstorff, and M. J. Gomes, "Effect of annealing temperature on photoluminescence and resistive switching characteristics of ZnO/Al_2O_3 multilayer nanostructures," J. Alloys Compd. **619**, 248–252 (2015).

[25] S. Rajarathinam, U. Ganguly, and N. Venkataramani, "Impact of oxygen partial pressure on resistive switching characteristics of PLD deposited $ZnFe_2O_4$ thin films for RRAM devices," Ceram. Int. **48**, 7876–7884 (2022).

[26] A. Li, Q. Li, C. Jia, and W. Zhang, "Control of resistive switching type in $BaTiO_3$ thin films grown by high and low laser fluence," Appl. Phys. Lett. **122**, 232104 (2023).

[27] S. Lamichhane, S. Sharma, M. Tomar, and A. Chowdhuri, "Impact of laser energy on resistive switching properties of $BiFeO_3$ thin films," Mater. Chem. Phys. **293**, 126824 (2023).

[28] R. Kumar, G. Kumar, and A. Umar, "Pulse laser deposited nanostructured ZnO thin films: A review," J. Nanosci. Nanotechnol. **14**, 1911–1930 (2014).

[29] R. K. Abdulnabi, M. H. Mohsin, R. A. Ismail, A. M. Mousa, and M. F. Jawad, "Effect of laser energy on the properties of nanostructured lead iodide film prepared via pulsed laser deposition technique," Optik **176**, 206–213 (2019).

[30] Y. Liu, N. Jiang, Y. Liu, D. Cui, C.-F. Yu, H. Liu, and Z. Li, "Effect of laser power density on the electrochromic properties of WO_3 films obtained by pulsed laser deposition," Ceram. Int. **47**, 22416–22423 (2021).

[31] A. I. Khudiar and A. M. Ofui, "Effect of pulsed laser deposition on the physical properties of ZnO nanocrystalline gas sensors," Opt. Mater. **115**, 111010 (2021).

[32] C. Funck and S. Menzel, "Comprehensive model of electron conduction in oxide-based memristive devices," ACS Appl. Electron. Mater. **3**, 3674–3692 (2021).

[33] K.-H. Xue, P. Blaise, L. Fonseca, G. Molas, E. Vianello, B. Traoré, B. De Salvo, G. Ghibaudo, and Y. Nishi, "Grain boundary composition and conduction in HfO_2: An ab initio study," Appl. Phys. Lett. **102**, 201908 (2013).

[34] Z.-Z. Jiang, Z. Guan, N. Yang, P.-H. Xiang, R.-J. Qi, R. Huang, P.-X. Yang, N. Zhong, and C.-G. Duan, "Epitaxial growth of $BiFeO_3$ films on $SrRuO_3$/$SrTiO_3$," Mater. Charact. **131**, 217–223 (2017).